ADDITIVE MANUFACTURING OF HYDRAULIC COMPONENTS – PRESSURE LOSS COMPARISON OF DIFFERENT SELF-SUPPORTING CHANNEL GEOMETRIES

Zita Tappeiner[1]*, Michiel Donners[1], Matthias Schmid[1], Katharina Schmitz[1]

[1]*Institute for Fluid Power Drives and Systems, RWTH Aachen University, Campus-Boulevard 30, 52074 Aachen*

* Corresponding author: Tel.: +49 241 8047729; E-mail address: zita.tappeiner@ifas.rwth-aachen.de

ABSTRACT

Additive manufacturing (AM) and in particular laser powder bed fusion (LPBF) are increasingly being used as manufacturing technology in hydraulics for flow optimization, function integration and weight reduction. These advantages can especially be exploited in hydraulic manifolds. Conventional manifold intersections are created by crossing two vertical bores. The turbulence resulting from the sharp edges and the deflection leads to undesired flow losses. These can be avoided with the design freedom of LPBF, which allows flow optimization in hydraulic channels. However, the development of new channel geometries is limited by design guidelines. Starting from a straight, round channel geometry, this paper presents the steps to design self-supporting channel geometries for horizontal build up. Therefore, different cross-sectional shapes are tested, and critical design details are explained. In addition, this paper examines the influence of post-processing methods on AM components. A comparison of the different geometries is shown with a CFD simulation as well as FEM simulation for strength investigation. For experimental investigation and simulation validation, selected test specimens were printed and post-processed. With a new designed test rig, the pressure losses of the different geometries and post-processing methods were measured and a comparison with the simulative results is shown. Overall, this paper provides an overview of the necessary steps in the design of hydraulic AM components for flow optimization.

Keywords: Additive Manufacturing, Laser Powder Bed Fusion, Flow Optimization, Design, 316L

1. INTRODUCTION

Components for hydraulic applications are mostly manufactured using conventional manufacturing processes, such as drilling and milling. Accordingly, manifold intersections are usually arranged at 90° to each other and dead volumes occur. Optimized positioning of the channels is possible, but the channel course can only be changed to a limited extent due to the tool geometry and is therefore mostly straight. [1–3]

The use of additive manufacturing (AM) for hydraulic components opens up many new advantages. First of all, structurally optimized components can be designed. This leads to an increase in efficiency due to the weight reduction in moving applications and enables a general material saving. Material resources and component weight can thus be saved. In addition, components can be designed with optimized flow. Flow-optimized channels can reduce pressure losses in the lines and thus save energy. An additional advantage is the functional integration that can be achieved through AM. This means that additional components can be saved, or the design can be adapted to desired functions. Due to these advantages, AM is of increasing importance in the production of hydraulic components, in particular in the production of manifolds [4–8]. Especially the targeted optimization of manifolds in

terms of flow and weight, while maintaining strength, is the subject of numerous research projects [9–13]. The aim of the latest studies is to automate the design process. After entering boundary conditions, entire manifolds can be automatically optimized and designed for AM [14]. For this new way of developing components, new design guidelines will be made available to serve as a template for the design of AM components. [15] Some of these guidelines are even specifically adapted to manifolds. [16] However, neither these guidelines nor the "Design for additive Manufacturing" (DfAM) [17] provide concrete rules for individual case decisions [18]. For example, if a circular cross-sectional area is not horizontally printable, various self-supporting channel geometries are available. In many publications, however, the decision process for a specific shape is not comprehensible or can only be applied to a few applications. This paper therefore aims to provide basic design recommendations for the design of hydraulic channels. As an example, the material 316L (1.4404) is treated in this study. Therefore, statements on material properties refer specifically to this material, but are often transferable to other materials.

1.1. Additive Manufacturing and post-processing

The manufacturing process studied in this paper is Laser Powder Bed Fusion (LPBF). The Fraunhofer Institute for Laser Technology [19] in Aachen played a key role in developing this process, which was patented back in 1996 [20]. LPBF is based on the layer-by-layer melting and subsequent solidification of components from metal powder. Components can thus be generated directly from a digital model. In this way, components with complicated geometries can be manufactured that cannot be realized using conventional methods [21].

Conventional manufacturing processes usually result in uniform microstructures, whereas additive manufacturing (AM) parts typically exhibit noticeable porosity and increased surface roughness [22]. However, the results depend largely on the specific printing parameters. Key factors such as printing direction, laser parameters, porosity, defects, surface finish, and subsequent heat treatment affect the mechanical properties of the material.

Likewise, the post-processing influences on material parameters. For example, the thermal post-processing method hot isostatic pressing (HIP), leads to increased density by eliminating porosity [23]. However, the thermally post-treated components only achieve lower yield strength compared to the as-printed samples. In contrast, a significant increase is observed in the maximum elongation and in ductility [24]. High temperatures can relieve residual stresses in the component and eliminate the direction-dependent properties from applying the material layer by layer. The microstructure is homogenized by the high temperature so that there are no longer melt pool boundaries [25]. Abrasive Flow Machining (AFM), a process for precise surface enhancement, can be used as a post-processing step after LPBF to improve surface quality. In the AFM process, viscoelastic polymers loaded with abrasive particles are passed through voids or channels to mitigate the inherently rough surface finish of untreated components [26]. For hydraulic applications, the target roughness values are typically around 0,4 µm [27]. In fluid dynamics, increased surface roughness results in pressure losses and therefore increased energy losses, reducing overall system efficiency [28]. When AFM is combined with HIP, further enhancements can be expected [29]. Rösler's comprehensive study [30] compared AFM with alternative methods, including vibratory finishing, sandblasting, chemically assisted vibratory finishing, and wet blasting. The investigation revealed that chemically assisted vibratory finishing (AFM) effectively reduced the R_a value from 10 µm to 0,7 µm, offering a cost- and time-efficient approach. In addition, AFM can improve the mechanical properties and lifetime of channels manufactured by the LPBF process. Increased internal surface roughness leads to the development of cracks, which negatively affects fatigue strength [31].

1.2. Comparison concept for channel geometries

A radius of a pipe or channel is often used to calculate flow parameters in a hydraulic system. This radius is known if a channel is circular but can also be calculated if the channel-shape differs from this. In this case, the hydraulic diameter can be described according to (1). It is calculated by multiplying the surface of the channel by 4 and dividing it by the circumference. This formula can be applied in turbulent flows (Re>2300) but is practically used in laminar flows as well, to analytically calculate and describe non-circular channels, although the invalidity of the formula in this state of flow. This formula offers a possible calculation to describe non-circular channels, which are mainly being investigated in this paper.

$$D_{hyd} = \frac{4A}{U} \tag{1}$$

Because of the invalidity of this formula in laminar flows, two other concepts for comparing different geometries are introduced in **Figure 1**. One approach for comparability is to keep the cross-sectional area constant. With constant volume flow, this would lead to constant average velocities. However, considering the transition to the round fitting geometry, it is difficult to keep the cross-sectional area constant over the entire length of the structure. The last option, which will be further pursued in this work, is a constant inner circle of the geometries. This method leads to as little influence on the run-in flow profile as possible.

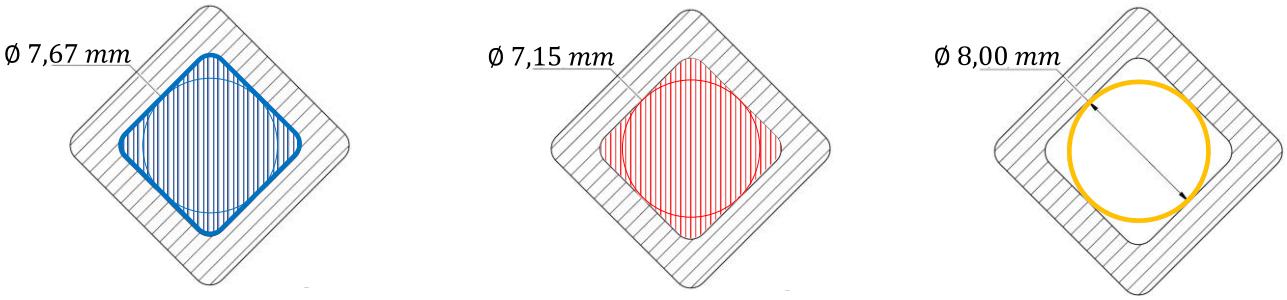

Figure 1: Different comparison criteria for the non-circular geometries

1.3. Channel Geometries for AM

Circular channels exceeding an inner diameter of 8 mm cannot be produced by LPBF without using inner supporting structures [32]. To solve this problem, the shape of the channel is being changed because greater diameter is often being used in hydraulic applications to reduce average flow speeds. Schmelzle et al. applied a diamond-shaped channel-section and were able to reduce weight by 60%. They compared a droplet shape to a diamond shaped channel and found that symmetrical channel geometries are the most material efficient compared to unsymmetrical shapes (like a drop) [10]. Alshare et al. reduced pressure losses by 21% and weight by 84% [11]. DIN EN ISO/ASTM 52911-1 suggests a droplet shape as an alternative to circular but does not standardize this shape for hydraulic applications [32]. In this proposal, a 90° rectangular roof is positioned on three fourths of a circle, where the overhang angle exceeds 45°, as can be seen in **Figure 2**.

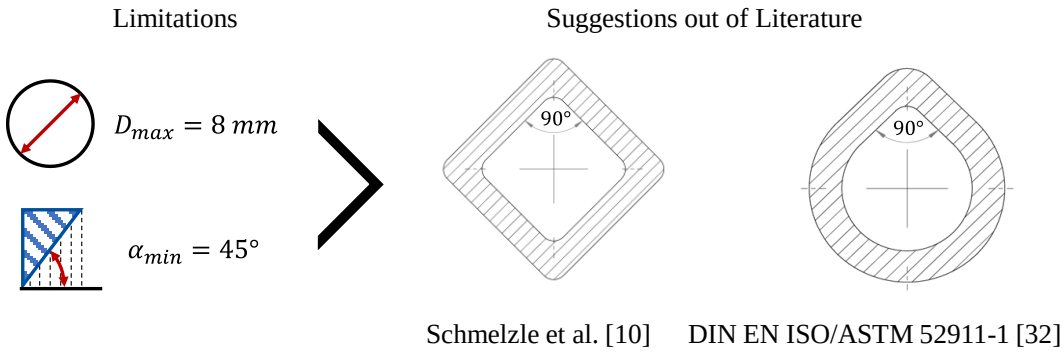

Figure 2: Limitations and suggestions for channel design

1.4. Topology of additively manufactured components

In addition to the advantages regarding flow optimization, the AM offers great potential regarding weight savings, especially in the application of hydraulic circuits. After designing the inner contour, the outer contour must be determined for the specimens. In the simplest case, a geometry with estimated constant wall thickness is evaluation by FEM to meet load requirements. However, the aim is also to optimize the wall thickness depending on the load. For the manufacturing process as such, the wall thickness required by the design is particularly relevant for the duct geometries. In contrast to the case of a round pipe, the modified duct geometries have an inhomogeneous stress distribution at constant pressure load. The stress distribution is the starting point for the design measures to avoid failure. In the process of topology optimization, the reduction approach is followed. The initial geometry of the component is therefore over dimensioned. The stress distribution is determined in the FEM with the meshed model. Iteratively, model elements with uncritical stress values are eliminated. This results in successively reduced nominal geometry [33]. For the special application case regarding additively manufactured components, the anisotropy of the material is also of great importance. The direction of manufacturing affects the subsequent expansion behavior of the channel geometries [34]. However, due to the rectified component alignment in the manufacturing process, this aspect is not initially considered here and compensated for by the safety factor.

2. METHODS

To compare different cross-sectional areas, four different shapes are selected and first optimized simulatively in terms of flow and strength. Three test specimens were manufactured from each geometry using LPBF with 316L. Thus, a total of twelve test specimens were printed, of which four remained untreated, four were post-treated by the HIP method, and four were post-treated by the AFM method. In subsequent bench tests, the pressure difference generated by the test specimens was measured and compared with the simulated results.

2.1. Design Process

In this work, three alternatives to a circular shape were investigated. A triangular and a quadratic shape are investigated because of their symmetrical shape, which are the most material efficient due to a homogeneous distribution of stress [10]. A symmetrical pentagonal or hexagonal shape cannot be printed in a horizontal build orientation because of the overhang angle at the top exceeding the maximal printable angle of 45° [35, 36]. As a third concept, a droplet shape, is compared to a circular shape because the DIN EN ISO/ASTM 52911-1 suggests this form as an alternative to a circular channel geometry [32]. The sharp edges occurring in the alternative shapes are rounded off, to prevent tension maxima.

A round cross-section with a diameter of 8 mm is chosen as the object of comparison. A diameter of 8 mm is the largest possible round cross-section for additive manufacturing in the horizontal mounting direction. The constant inner diameter enables a connection between the investigated and the circular shape without cross-section narrowing for the run-in flow profile, which also enables easier machining. The second concept is based on a constant hydraulic diameter of 8 mm, which is calculated out of the inner surface and circumference. The inner diameter decreases compared to concept one, by equalizing a hydraulic diameter of 7,67 mm. This concept is most logical from a theoretical perspective because this formula is most used to calculate divergent shapes of circular. In the third and last concept, the average speed of flow is constant, by equalizing the inner surface to a circular channel. Hereby, the inner diameter further reduces in size compared to concept one and two. To influence the run-in flow as little as possible, the first concept with a constant inner diameter is chosen as the comparison criterion in this work.

The connection between the investigated channel geometries and the circular connection to the hydraulic system is being constructed by a straight phase at an angle of 45 degrees perpendicular to the building platform. The occurring sharp edges are smoothened out with a radius of 1 mm to reduce stress maxima and improve flow efficiency. These concepts of dimensioning are combined with the connection and are constructed into test parts, which are being investigated in a test rig, to validate the simulated results of the CFD- and FEM-simulations. These results should bring insight into an optimal channel geometry for hydraulic applications, considering mechanical and flow parameters. The geometry of the transition and the shape of the square specimen are shown in **Figure 3**.

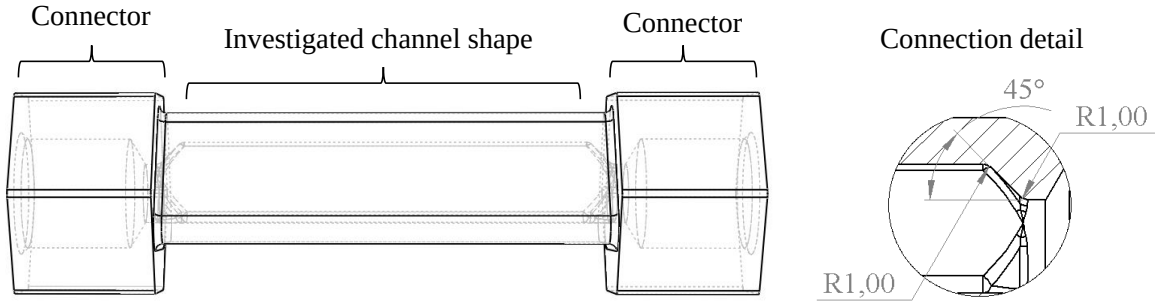

Figure 3: Transition from round cross-section to self-supporting channel geometry

Four test parts were produced three times repetitively to post-process differently (no post-processing, HIP, AFM). The four test parts consisted of the same connector at both ends and the connection between the circular and investigated channel geometry. In the middle of the test part, a circular, triangular, rectangular, and droplet-shaped channel geometry was constructed into the final test parts. CFD- and FEM-results were taken into review to select an optimal concept for dimensioning the inner diameter of the middle section.

2.2. CFD-Simulation

Computational Fluid Dynamics simulations (CFD) were applied to bring insight into the flow characteristics of the test parts. The pressure loss and streamlines were mainly investigated and optimized. In this work, Ansys Fluent software was used to bring these insights. The mesh was constructed with an element size of 0,48 mm, an inflation layer of 0,4 mm and a growth rate of 1,2 divided into 16 layers. These parameters are based on experiences and on Zardin et al. [2]. They found that a ratio of element size to diameter should not exceed 0,06 to ensure realistic results. An ISO VG 46 mineral oil was used in the test setup and modelled in the simulations, which is often used in hydraulic applications. To simulate the oil flowing through the test part, an inlet, an outlet, and a wall are defined. A fully developed flow is specified at the inlet with a velocity inlet. The simulated

corresponds with the analytical profile. At the outlet, a pressure outlet is specified at a static pressure of 150 bar, which corresponds to the operating point. A turbulent intensity of 6.78% was specified at the in- and outlet, as can be calculated out of formula (2). A no-slip condition and an average roughness height of $15 \cdot 10^{-6}$ m were specified to model the rough surface of the as-built test parts. The numerical coupled scheme with a Green-Gauss cell-based gradient and a second order discretization were used to ensure realistic results, with a residuum of 10^{-6} that acted as the criterion of convergence. The SST-k-omega model combined with the Low Reynolds Number Correction was used, after comparing the values of pressure losses of different models (like k-epsilon and laminar) to the analytical pressure loss of a pipe. These settings were used to simulate all concepts and gain insight into the flow characteristics of the test parts [37].

$$I = 0{,}16 \cdot Re^{-1/8} \tag{2}$$

The influence of the post-processing methods is not considered in the simulation, but the wall roughness is only adapted to literature values for the surfaces of additively manufactured components. Since the flow condition in the components is laminar at the operating point of 150 bar and 16,5 l/min (operating point for the comparison), the roughness theoretically does not have a large influence on the pressure drop. The consideration of the generated surface values will be part of further research.

2.3. FEM-Simulation

A Finite Element Method simulation (FEM) is used to determine the wall thicknesses of the channel geometries. In this publication, the outer diameter and corner radius were varied in 80 combinations. An optimization, for findings the lightest combination, that also exceeds the safety margins was conducted. The safety factor of 1,7 is based on DIN 2413 [38], which is applied to calculate wall thicknesses of pipes in hydraulic applications. The results of the design study have been validated in Ansys Mechanical, which confirmed the choice of varying the outer diameter and corner radius. **Figure 4** shows that maximum tensions according to Von Mises occur in these spots. The wall thickness increases from the droplet to the squared and triangle shaped sections. This, of course, increases the weight and outer circumference of the channel sections and increases building time and costs, which represents a disadvantage.

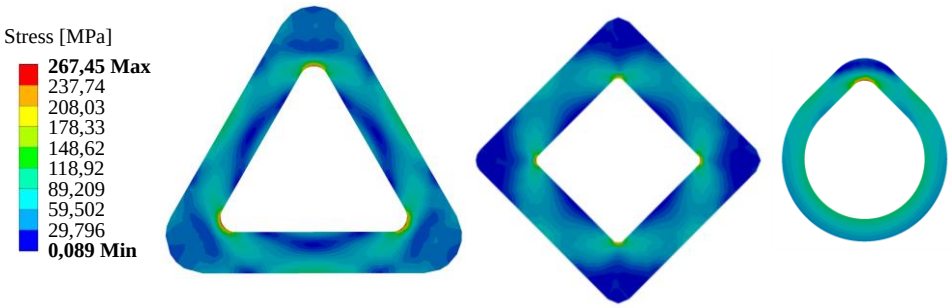

Figure 4: Stress within the components

Based on the results of the FEM, a topology optimization is carried out. Since the FEM already provides a resilient geometry with constant wall thickness from manually run through steps, this is taken as the starting point. An estimation on a round channel using Barlow's formula gives an alternative reference value to reasonably choose the initial value of the wall thickness. Especially when new geometries are to be developed that have not yet passed through any elaborate FEM loops. This ensures that the solution converges reliably. Due to the inhomogeneous stress distribution in the drop-shaped channel geometry, the geometry is divided into several sections, for each of them the meshing is done independently. Especially in the area of the tip of the drop geometry, a considerable mesh refinement is carried out. A study carried out here shows that an element size of 20% of the

initial wall thickness should not be exceeded and at the same time, the limit of the absolute size of maximum 0,1 mm edge length of the elements should be kept. Preferably, a homogeneous hexahedral meshing within the individual sectors is used. This leads to valid results and reflects the discretization of the wall thickness in a comprehensible way. The target value is the inner contour of the pipe geometry. Therefore, it is fixed as a conservation variable in the bearing. Consequently, the front side is also fixed as a fixed bearing. The original wall thickness is preserved and leads to a load-bearing structure.

2.4. Post-processing parameters

After fabrication, the specimens were sawed off the build plate and all external support structures were removed. Four of the test specimens were left as-built and only machined on the functional surfaces so that they could be bolted to the test rig.

One third of the specimens were reworked using the HIP process. In this process, the specimens were subjected to a temperature of 1150°C and a pressure of 1000 bar for 4 hours. During the process, the specimens are surrounded by argon. The final operating point was ramped and cooling and pressure reduction occurred slowly over a period of 4 hours.

Another third of the specimens, each with one of the different geometries, was subjected to grinding post-treatment. The AFM method was used for this purpose. The grain material of the medium used was aluminum zirconia with a grain size of mesh 24/36. The viscosity was classified to 2227,72 Pa·s, measured at 1 rad/s. Flow grinding was performed for 24 minutes at 65 bar.

2.5. Test Rig

On the test rig used for the experimental investigation, the test specimens can be screwed in between two adapters. **Figure 5** shows the hydraulic circuit diagram of the test rig. The pressure is adjusted to 150 bar via the proportional valve (1). The cooler (2) is temperature controlled and regulates the operating temperature to 40°C. The flow rate is set to 16,5 l/min via the pump (3). A differential pressure sensor (4) measures the pressure drop across the specimen. After reaching steady state, for all specimens the pressure loss is recorded.

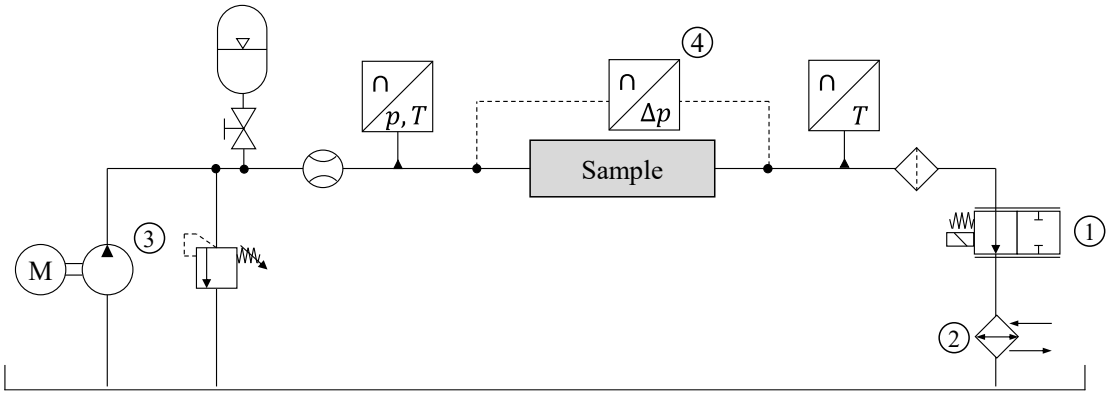

Figure 5: Hydraulic circuit diagram of the test bench

3. RESULTS

With the help of the CFD and FEM results, the final shapes of the components have been designed. The results of the simulations were particularly decisive for the selection of the shape, the course of the cross-section transition and the choice of wall thickness. The strength of the components was confirmed on a test rig by a static compression test at 165 bar (10% above the operating pressure). All components exhibited the necessary strength.

3.1. CFD-Results

The simulated pressure losses of the different geometries are listed in the second column of **Table 1**. In addition, **Figure 6** shows the flow lines within the channels for the triangle, square, and drop.

Table 1: Simulation results of the specimens

Form	Pressure loss Δp [bar]	Cross-sectional area A [mm²]	Wall thickness t [mm]
Circle	0,17741	50,625	0,3
Square	0,15076	63,142	1,5
Triangle	0,14643	81,084	2,75
Drop	0,16920	53,479	1,25

The flares at the inlet and outlet of the components are caused by the thread runout of the fittings. Since only the inside is shown, the 8 mm inner diameter of the screw-in fitting can be seen at the inlet. However, since the hydraulic fitting is not flush with the end of the bore, the cross-sectional expansion occurs. Dead volumes are created at these points. Additional dead volumes occur at the transition from the round 8 mm cross-section to the self-supporting channel contour. Due to the larger cross-sectional area, this effect is particularly strong in the triangle.

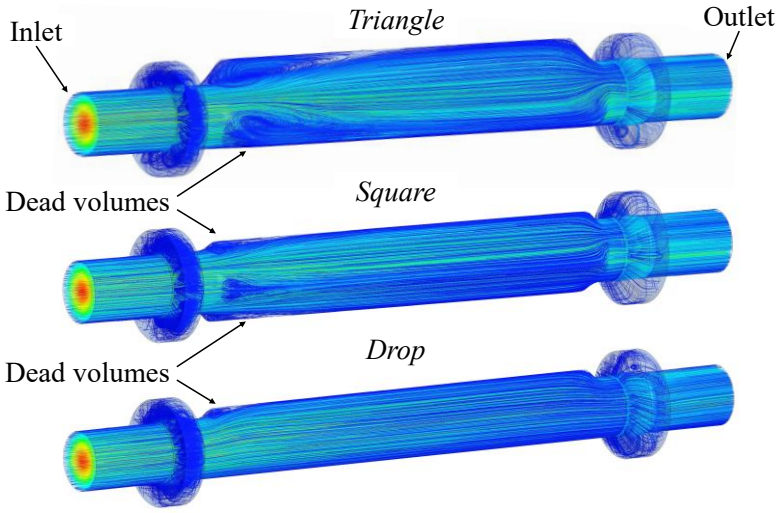

Figure 6: Simulation of the flow lines in the non-circular cross-sectional shapes

3.2. FEM-Results

With the aid of FEM simulation, a suitable wall thickness was developed for each geometry, at which the maximum stress in the component is not exceeded, considering the safety factor. These wall thicknesses, also listed in Table 1, differ for the various shapes. The highest wall thickness is required for the triangle since significant stress peaks form at the corners. The most suitable shape in terms of stress is the circle, which requires a wall thickness of only 0,3 mm. However, such thin walls cannot be printed with the selected manufacturing process, which is why the wall thickness was increased to 2 mm for this component. This corresponds to the wall thickness of a standard 12S tube. In order to make a prediction about possible weight savings, a topology optimization was carried out in this work. The resulting geometries will also be used for future static compression tests. The right side in **Figure 7** shows an example of the reduced geometry of a drop shape because of topology optimization without a safety factor. The stress state in the detail of the tip is shown opposite. From this, the material accumulation in this geometry section is derived.

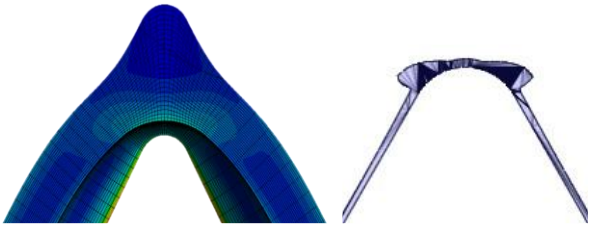

Figure 7: Topology optimization upon of drop shape

Due to the inhomogeneous wall thickness over the circumference, only a rudimentary estimation is possible at first. As expected, there is an accumulation of material at the tip of the drop. In order to be able to give a holistic assessment, a comparative value to the original geometry is used. The cross-sectional area of the resulting wall is determined and compared with the result determined in the same way for a channel with a round cross-section. This results in a new average wall thickness. Compared to the round duct, this results in a weight reduction of 16%.

3.3. Experimental results

The results of the experimental (filled markers) and simulative (unfilled markers) investigation are shown in **Figure 8**. For each component geometry, the pressure drop is plotted for the untreated, the thermally post treated and the AFM-treated component. Differences between the various geometries can be seen. The post-treatment processes also lead to a change (mostly a reduction) in the pressure difference for all components except the triangle.

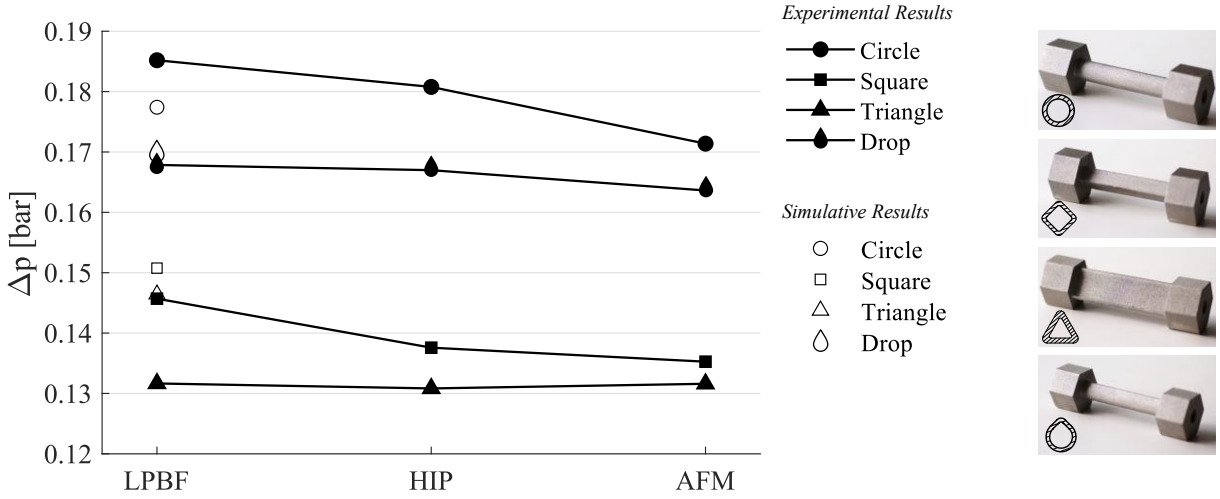

Figure 8: Measured pressure loss of different geometries and post-processing methods

The designed components could all be built horizontally without support structures in the channels and no leakage occurred in the hydraulic application. A static pressure test proofed, that the specimens can withstand a pressure of 150 bar and even 165 bar did not cause any leakage. In the round shape, a clearly discernible difference in quality occurred on the downward-facing surface. Here, there was a collapse of the shape and a significantly increased roughness. This confirms that the use of the round cross-section is not recommended for diameters above 8 mm.

The HIP process only has an influence on the pressure difference for the round and square shapes. The AFM method shows more effect on pressure loss reduction. Except for triangle shapes, the pressure difference generated by the component decreases for all shapes compared to the unprocessed parts. A connection to the flow lines in Figure 6 can be recognized. In the case of the triangle, a particularly large dead volume occurs and, due to the larger cross-sectional area, the velocity inside the component decreases under constant volume flow. Accordingly, the grind effect of the abrasive

medium is lower here. In the round shape, the flow is fastest and without dead volume, so that the greatest effect can be achieved. It should be noted that the AFM process was applied before the machining post-processing, so that the entry channel into the component was still at 8 mm and there was no widening as in Figure 6 at the transition to the round fitting-geometry. In the case of the non-circular geometries, this resulted in the highest material removal occurring precisely in this area, which was later partially widened.

4. DISCUSSION

The experimental results confirm the simulation because the rank order of the geometries was predicted correctly. Comparing the different geometries, a round geometry causes the highest pressure loss. However, this must be evaluated considering the comparison criterion of constant inner diameter. Consequently, the cross-sectional area also has to be taken into account. The constant inner diameter leads to a higher cross-sectional area for non-circular shapes. The pressure loss corresponds with the cross-sectional area. However, the relationship is not proportional. Accordingly, a constant cross-sectional area would not have led to constant pressure differences. The constant inner circle as a comparison criterion is more suitable for obtaining a run-in flow profile and is therefore appropriate for comparison here. In terms of post-processing, the trends are the same for almost all components. Since the HIP process is not usually used for external post-processing, but to change the material properties, there is no significant change in the pressure loss in the samples. However, since very high temperatures occur during the process, it is possible that individual splashes or powder residues are melted and change their surface properties.

5. CONCLUSION AND OUTLOOK

In this paper, the fundamentals for the use of LPBF in hydraulic applications were determined. Starting with an iterative CFD simulation, a transition from the connection geometry to a self-supporting shape was designed. FEM was then used to determine a suitable wall thickness for the various geometries. In bench tests, all components have proven their strength and leak proofness. In addition, the measured values showed that the CFD simulation was correctly designed, and the predicted sequence of shapes was correct. Thus, the test rig and simulation settings can be used for further studies on additively manufactured components. Whether the constant inner diameter is the correct comparison criterion depends on the application. If the flow is to be kept as constant as possible without turbulence, then it is a suitable criterion. If the installation space is limited, a constant cross-section would be more suitable. Another approach would be to use a constant amount of material, but this would result in much smaller cross-sections for the non-circular shapes, since these require greater wall thicknesses. The HIP and AFM methods have demonstrated their effectiveness in reducing pressure loss. However, both have only been tested in a single parameter combination and can be further refined in targeted experiments. In particular, widening of the channel should be avoided for grinding.

The aim of further research is to investigate more complex channel courses. With the knowledge gained from the linear test specimens, further investigations of three-dimensional channel courses can be carried out. In this context, a general methodology should be developed that offers solutions for various requirements. For non-round shapes, for example, the orientation of the shape in curves will become relevant. In addition, the roughness of the components should be determined and integrated into the simulation.

ACKNOWLEDGEMENTS

This research and development project is funded by the Federal Ministry for Economic Affairs and Climate Action (BMWK) within the Technologietransfer-Programm Leichtbau (TTP LB) and supervised by Projektträger Jülich.

NOMENCLATURE

A	Cross-sectional area	[m²]
AFM	Abrasive Flow Machining	
AM	Additive Manufacturing	
CFD	Computational Fluid Dynamics	
DfAM	Design for Additive Manufacturing	
D_{hyd}	Hydraulic diameter	[m]
FEM	Finite element Method	
HIP	Hot Isostatic Pressing	
LPBF	Laser Powder Bed Fudion	
Δp	Pressure difference	[bar]
U	Area perimeter	[m]

REFERENCES

[1] Chambon, R., Tollenaere, M. (1991) Automated Al-based mechanical design of hydraulic manifold blocks. Computer-Aided Design:213–222

[2] Zardin B, Cillo G, Rinaldini C et al. (2017) Pressure Losses in Hydraulic Manifolds. Energies 10:310. https://doi.org/10.3390/en10030310

[3] Zhang J, Liu G, Ding R et al. (2019) 3D Printing for Energy-Saving: Evidence from Hydraulic Manifolds Design. Energies 12:2462. https://doi.org/10.3390/en12132462

[4] Semini C, Goldsmith J, Manfredi D et al. (2015) Additive manufacturing for agile legged robots with hydraulic actuation. In: 2015 International Conference on Advanced Robotics (ICAR), pp 123–129

[5] Pietropaoli M, Ahlfeld R, Montomoli F et al. (2017) Design for Additive Manufacturing: Internal Channel Optimization. Journal of Engineering for Gas Turbines and Power 139. https://doi.org/10.1115/1.4036358

[6] Diegel O, Schutte J, Ferreira A et al. (2020) Design for additive manufacturing process for a lightweight hydraulic manifold. Additive Manufacturing 36:101446. https://doi.org/10.1016/j.addma.2020.101446

[7] Rekadze P, Rodionov L, Satsyuk I (2018) Analysis of hydraulic units manufactured by powder bed fusion. In: 2018 Global Fluid Power Society PhD Symposium (GFPS)

[8] Zhang C, Wang S, Li J et al. (2020) Additive manufacturing of products with functional fluid channels: A review. Additive Manufacturing 36:101490. https://doi.org/10.1016/j.addma.2020.101490

[9] Chekurov S, Lantela T (2017) Selective Laser Melted Digital Hydraulic Valve System. 3D Printing and Additive Manufacturing 4:215–221. https://doi.org/10.1089/3dp.2017.0014

[10] Schmelzle J, Kline EV, Dickman CJ et al. (2015) (Re)Designing for Part Consolidation: Understanding the Challenges of Metal Additive Manufacturing. Journal of Mechanical Design 137. https://doi.org/10.1115/1.4031156

[11] Alshare AA, Calzone F, Muzzupappa M (2019) Hydraulic manifold design via additive manufacturing optimized with CFD and fluid-structure interaction simulations. RPJ 25:1516–1524. https://doi.org/10.1108/RPJ-03-2018-0064

[12] Geating JT, Wiese MC, Osborn MF (2017) Design, fabrication, and qualification of a 3d printed metal quadruped body: combination hydraulic manifold, structure and mechanical interface. 2017 International Solid Freeform Fabrication Symposium

[13] Zhu Y, Wang S, Zhang C et al. (2020) AM-driven design of hydraulic manifolds: enhancing fluid flow and reducing weight. In: 12th International Fluid Power Conference, pp 155–159

[14] Biedermann M, Beutler P, Meboldt M (2021) Automated design of additive manufactured flow components with consideration of overhang constraint. Additive Manufacturing 46:102119. https://doi.org/10.1016/j.addma.2021.102119

[15] Kumke M (2018) Methodisches Konstruieren von additiv gefertigten Bauteilen. Dissertation, Technische Universität Braunschweig

[16] Rolinck N, Schmitt M, Schneck M et al. (2021) Development Workflow for Manifolds and Fluid Components Based on Laser Powder Bed Fusion. Applied Sciences 11:7335. https://doi.org/10.3390/app11167335

[17] Godec D, Gonzalez-Gutierrez J, Nordin A et al. (2022) A Guide to Additive Manufacturing. Springer International Publishing, Cham

[18] Laverne F, Segonds F, Anwer N et al. (2015) Assembly Based Methods to Support Product Innovation in Design for Additive Manufacturing: An Exploratory Case Study. Journal of Mechanical Design 137. https://doi.org/10.1115/1.4031589

[19] Alfaify A, Saleh M, Abdullah FM et al. (2020) Design for Additive Manufacturing: A Systematic Review. Sustainability 12:7936. https://doi.org/10.3390/su12197936

[20] Meiners W, Wissenbach K, Gasser A (1996) Verfahren zur Herstellung eines Formkörpers

[21] Kumar S (2022) Additive Manufacturing Solutions. Springer International Publishing AG, Cham

[22] Haghdadi N, Laleh M, Moyle M et al. (2021) Additive manufacturing of steels: a review of achievements and challenges. J Mater Sci 56:64–107. https://doi.org/10.1007/s10853-020-05109-0

[23] Maier HJ, Niendorf T, Bürgel R (2019) Handbuch Hochtemperatur-Werkstofftechnik: Grundlagen, Werkstoffbeanspruchungen, Hochtemperaturlegierungen und -beschichtungen, 6., überarbarbeitete und erweiterte Auflage. Springer Vieweg, Wiesbaden, Heidelberg

[24] Liverani E, Lutey AHA, Ascari A et al. (2020) The effects of hot isostatic pressing (HIP) and solubilization heat treatment on the density, mechanical properties, and microstructure of austenitic stainless steel parts produced by selective laser melting (SLM). Int J Adv Manuf Technol 107:109–122. https://doi.org/10.1007/s00170-020-05072-9

[25] Grech IS, Sullivan JH, Lancaster RJ et al. (2022) The optimisation of hot isostatic pressing treatments for enhanced mechanical and corrosion performance of stainless steel 316L produced by laser powder bed fusion. Additive Manufacturing 58:103072. https://doi.org/10.1016/j.addma.2022.103072

[26] Gillespie LK (1999) Deburring and edge finishing handbook. Society of Manufacturing Engineers; American Society of Mechanical Engineers, Dearborn, Mich., Fairfield, NJ

[27] Matthiesen G, Merget D, Pietrzyk T et al. (2020) Design and experimental investigation of an additive manufactured compact drive. In: 12th International Fluid Power Conference, pp 137–147

[28] Kumar SS, Hiremath SS (2016) A Review on Abrasive Flow Machining (AFM). Procedia Technology 25:1297–1304. https://doi.org/10.1016/j.protcy.2016.08.224

[29] Duval-Chaneac MS, Han S, Claudin C et al. (2018) Characterization of maraging steel 300 internal surface created by selective laser melting (SLM) after abrasive flow machining (AFM). Procedia CIRP 77:359–362. https://doi.org/10.1016/j.procir.2018.09.035

[30] Rösler Oberflächentechnik (2020) Innenkanäle effizient und automatisiert bearbeiten. J Oberfl Techn 60:54–57. https://doi.org/10.1007/s35144-020-0999-z

[31] Yu C-H, Leicht A, Peng RL et al. (2021) Low cycle fatigue of additively manufactured thin-walled stainless steel 316L. Materials Science and Engineering: A 821:141598. https://doi.org/10.1016/j.msea.2021.141598

[32] DIN Deutsches Institut für Normung e.V. (2019) Additive Fertigung - Konstruktion - Teil 1: Laserbasierte Pulverbettfusion von Metallen: DE_307153562(DIN EN ISO/ASTM 52911-1)

[33] Klein B (2003) FEM: Grundlagen und Anwendungen der Finite-Elemente-Methode, 5. Auflage. Vieweg+Teubner Verlag, Wiesbaden

[34] Qu S, Ding J, Fu J et al. (2022) Anisotropic material properties of pure copper with fine-grained microstructure fabricated by laser powder bed fusion process. Additive Manufacturing 59:103082. https://doi.org/10.1016/j.addma.2022.103082

[35] Thomas D (2009) The Development of Design Rules for Selective Laser Melting. Dissertation, University of Wales Institute, Cardiff

[36] Gibson I, Rosen D, Stucker B et al. (2021) Additive Manufacturing Technologies: Third Edition. SPRINGER NATURE, [S.l.]

[37] ANSYS (2023) Ansys Resource Center | Webinars, White Papers and Articles. https://www.ansys.com/resource-center#t=ResourceCenterTab&sort=relevancy&numberOfResults=50. Accessed 24 Apr 2023

[38] DIN Deutsches Institut für Normung e.V. (2020) Nahtlose Stahlrohre für öl- und wasserhydraulische Anlagen - Berechnungsgrundlage für Rohre und Rohrbögen bei schwellender Beanspruchung. Accessed 2020